INSTITUTE OF PHYSICS PUBLISHING JOURNAL OF PHYSICS D: APPLIED PHYSICS

J. Phys. D: Appl. Phys. **36** (2003) 1–8 PII: S0022-3727(03)57391-0

Short pulse laser propagation through tissues for biomedical imaging

Champak Das[1], **Ashish Trivedi**[1], **Kunal Mitra**[1,3] **and Tuan Vo-Dinh**[2]

[1] Mechanical and Aerospace Engineering Department, Florida Institute of Technology, 150 W. University Blvd., Melbourne, FL 32901, USA

[2] Oak Ridge National Laboratory, PO Box 2008, MS 6101, Oak Ridge, TN 37831-6101, USA

E-mail: kmitra@fit.edu and vodinht@ornl.gov

Received 12 December 2002, in final form 9 April 2003
Published
Online at stacks.iop.org/JPhysD/36

Abstract

An experimental and numerical study is performed to analyse short pulse laser propagation through tissue phantoms without and with inhomogeneities embedded in it. Short pulse laser probing techniques have distinct advantages over conventional very large pulse width or cw lasers primarily due to the additional information conveyed about the tissue interior by the temporal variation of the observed signal. Both the scattered temporal transmitted and reflected optical signals are measured experimentally using a streak camera for samples irradiated with a short pulse laser source. Parametric study involving different scattering and absorption coefficients of tissue phantoms and inhomogeneities as well as the detector position and orientation is performed. The temporal and spatial profiles of the scattered optical signals are compared with the numerical modelling results obtained by solving the transient radiative transport equation using discrete ordinates technique.

1. Introduction

Optical imaging of turbid media such as biological tissues is a difficult and challenging problem in modern optical technology due to overwhelming light scattering that severely reduces image contrast and degrades spatial resolution. In the last few years novel optical imaging methods have been developed to analyse interactions between near infrared light and biological tissues in order to monitor the physiological and morphological status of living tissues and organs without adverse side effects [1–10]. Optical tomography uses multiple sources and detectors placed on the tissue surface to map changes in the optical properties directly below the surface, or to form a simple projection in a transmittance geometry [11]. The simplest system is one that records the transmitted intensity at the surface in response to illumination by a continuous source (CW) of light. Although measurements of changes in intensity have been successfully employed by some researchers [6, 8, 12] it is not possible to distinguish between changes in absorption and changes in scatter. Furthermore, in the presence of unknown inhomogeneous scattering or absorbing background structure, localization and quantization of absorption changes may be erroneous [13].

Short pulse laser probing techniques for diagnostics have distinct advantages over very large pulse width or continuous wave lasers primarily due to the additional information conveyed by the temporal distribution of the observed signal [14, 15]. The distinct feature is the multiple scattering induced temporal distribution, which persists for a time period greater than the duration of the source pulse and is a function of the source pulse width as well as the optical properties of the medium. If the detection is carried out at the same short timescale (comparable to the order of the pulse width), the signal continues to be observed even at large times after the pulse has been off due to the time taken for the photons to migrate to the detector after multiple scattering in the media. Therefore in this paper for optical imaging, a short pulse laser is focused on the region to be probed and scattered reflected/transmitted signals are measured at different locations using streak camera.

Contrast and spatial resolution of optical imaging in turbid media is also performed by time gating techniques

[3] Author to whom correspondence should be addressed.

[9]. Short pulse laser and time-gated detection allows one to select photons that travel along comparatively short trajectories and suffer a correspondingly smaller number of scattering events. Pulses traversing through discrete scattering media is considered to be split into ballistic (coherent) and diffuse (incoherent) components [16]. If only the earliest arriving photons are collected by an appropriate gating technique, the direct line of sight property variations can be inferred since the earliest arriving photons correspond to those travelling the shortest optical path between the source and detector [17, 18]. The photons detected first have been deviated least from the optical axis and the intensity measured over a small period depends on the optical properties of the region contained within a small volume surrounding the optical axis. Time gating [19], space gating [20, 21], holographic gating or optical coherence interferometry techniques [22], and streak camera applications [23] have been used for evaluating the earliest arriving photons. However, these ballistic components may not be of practical use for tissues thicker than a few centimetres because they are not measurable with increasing tissue thickness. The significant drawback of time gating is that vast majority of transmitted light is discarded and the scarcity of detected photons with the shortest path lengths limits the achievable gain in resolution [24]. A further improvement in spatial resolution therefore relies on higher spatial resolution information being encoded within the available distribution of longer flight-time transmitted photons. Thus forward and backward radiative transport models for determination of optical properties of the tissue interior from transmitted and reflected signal measurements can therefore be based on the full temporal signal [25–27].

In addition to time resolved techniques, frequency domain techniques also commonly used for biomedical imaging is by measuring the demodulation and phase shift of transmitted light due to interaction of tissue medium with intensity modulated light source. A significant disadvantage of the frequency domain method, though generally a less expensive method, is that sources that can provide significant power at very high frequencies are not yet available. Most experimental works performed so far have utilized frequencies of a few hundred megahertz, which is equivalent to a temporal resolution of a few nanoseconds, and photon density wavelengths of the order of a metre [28–30]. It has been reported in the literature that there is a need for high modulation frequencies to obtain images with high resolution when imaging tissues having particularly low average absorption and high scattering coefficients [31].

In order to predict the optical properties of tissues from time-resolved scattered signal measurements development of inverse algorithm is required. Before development of complex inverse algorithms, accurate forward solutions of transient radiative transport equation (RTE) necessary to analyse short pulse laser propagation through tissues is critical. In most previous analysis, the transient term of the RTE is usually neglected. This assumption does not lead to errors as the temporal variations of observed signals are slow compared to the time of flight of a photon. However, in applications involving short pulse laser interactions with tissues, the transient effect must be considered in the RTE [14, 32, 33].

Transient solution of radiative transfer equation for one-dimensional geometry for the case of short pulse laser incidence has been developed and reported in the literature [14, 34–36]. The work has been extended to two-dimensional geometry using the simplified first order spherical harmonics (P_1) approximation for a rectangular geometry [37]. Integral equation formulation techniques for the transient RTE have been also developed [38, 39]. However, the P_1 model underestimates the speed of light propagation [14] and the integral formulation is difficult to be applied to complex geometries. Monte Carlo (MC) method has been also used by many researchers [40, 41]. The MC method requires a large number of emitted bundles to obtain smooth accurate solutions, which is computationally expensive. The discrete ordinate method (DOM) has become popular for solving transient RTE accurately and efficiently. The one-dimensional DOM has been used to analyse the transient radiant transfer in oceanographic liar. The DOM in conjunction with the piecewise parabolic method scheme used previously to obtain numerical solutions for two-dimensional scattering–absorbing medium is used in this paper [42].

No previous study has been reported in the literature which compares the experimentally measured scattered optical signals from a tissue medium containing inhomogeneities due to short pulse laser irradiation with accurate numerical solutions of transient RTE. Such studies are critical for predicting the optical properties of tissues from temporal scattered optical signal measurements. In this paper the temporal optical transmitted and reflected signals from tissue phantoms without and with inhomogeneities imbedded in it are measured with a streak camera. Parametric study involving different scattering and absorption coefficients of tissue phantoms and inhomogeneities as well as the detector position and orientation is performed. The experimentally measured temporal scattered optical signals are compared with numerical modelling results obtained by solving the transient RTE using the DOM

2. Mathematical formulation

In this paper the tissue base medium is approximated by an anisotropically scattering and absorbing rectangular enclosure in which an inhomogeneity is imbedded in it (see figure 1).

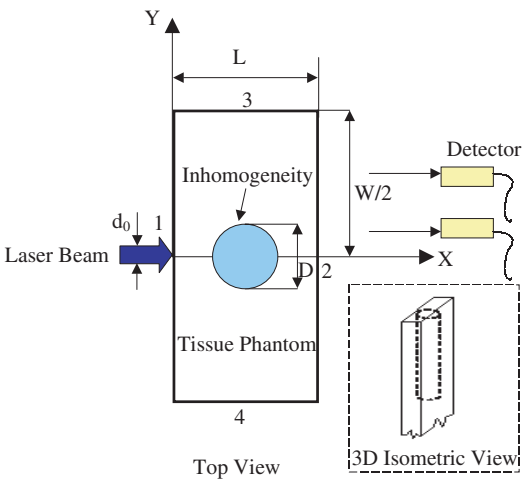

Figure 1. Schematic of the problem under consideration.

The transient radiative transfer equation in a given direction Ω is given by [14, 43]:

$$\frac{1}{c}\frac{\partial I(x,y,\Omega,t)}{\partial t}+\mu\frac{\partial I(x,y,\Omega,t)}{\partial x}+\eta\frac{\partial I(x,y,\Omega,t)}{\partial y}+k_e I(x,y,\Omega,t)=\frac{k_s}{4\pi}\int_{4\pi}\Phi(\Omega',\Omega)I(x,y,\Omega',t)\,d\Omega'+S(x,y,\Omega,t), \quad (1)$$

where I is the scattered diffuse intensity (W m^{-2} sr^{-1}), k_e and k_s are the extinction coefficient and the scattering coefficient, respectively, Φ the phase function, Ω the direction cosine, c the velocity of light in the medium, x and y are the spatial coordinates, t the time, and S is the source term.

The scattering phase function can be represented in a series of Legendre polynomials P_n by

$$\Phi(\Omega',\Omega)=\sum_{n=0}^{N}(2n+1)\,g^n P_n[\cos(\Theta)], \quad (2a)$$

where g is the asymmetry factor. The higher the value of g, the more forward scattered is the phase function of the medium. Tissues usually are highly forward scattered medium. The scattering angle $\Theta$is represented by

$$\cos(\Theta)=\mu\mu'+\eta\eta'+\xi\xi', \quad (2b)$$

where μ, η, and ξ are the direction cosines of the light propagation direction Ω.

The pulsed radiation incident on the tissue medium at face 1 (see figure 1) is a Gaussian-shaped pulse having a temporal duration (pulse width) t_p at full-width half-maximum (FWHM). The intensity can be separated into a collimated component, corresponding to the incident source, and a scattered intensity. If I_c is the collimated intensity, then I is the remaining intensity described by equation (1). The collimated component of the intensity for the square pulse is represented by

$$I_c(x,y,\Omega,t)=I_0\,e^{-k_e x}\left[H\left(t-\frac{x}{c}\right)-H\left(t-t_p-\frac{x}{c}\right)\right]\times\delta(\Omega-\Omega_0), \quad (3)$$

where I_0 is the intensity leaving the wall towards the medium, $H(t)$ the Heaviside step function, and $\delta(t)$ the Dirac delta function. The Gaussian pulse is approximated as a square pulse for ease of numerical implementation.

The source function S formed from the collimated irradiation is then given by

$$S(x,y,\Omega,t)=\frac{k_s}{4\pi}\int_{4\pi}\Phi(\Omega',\Omega)I_c(x,y,\Omega',t)\,d\Omega'. \quad (4)$$

The boundary conditions are such that intensity leaving the boundary surface is composed of the contribution of the outgoing emitted intensity and the reflection of incoming radiation in the direction Ω.

In the DOM, the radiative transfer equation and the associated boundary condition are replaced with a set of equations for a finite number of M directions that cover 4π sr solid angles. The integral terms of equations (1) and (4) are reformulated with the aid of an angular quadrature of order M.

The discrete form of the time-dependent RTE in the direction Ω_m is then represented as

$$\frac{1}{c}\frac{\partial I_m(x,y,t)}{\partial t}+\mu_m\frac{\partial I_m(x,y,t)}{\partial x}+\eta_m\frac{\partial I_m(x,y,t)}{\partial y}=-k_e I_m(x,y,t)+\frac{k_s}{4\pi}\sum_{m'=1}^{M}w_{m'}\Phi_{m'm}I_{m'}(x,y,t)+S_m(x,y,t), \quad (5)$$

where $m=-M,\ldots,-1,1,\ldots,M$, $\{\Omega_m, w_m\}$ defines a quadrature of M discrete directions Ω_m to which the weights w_m are associated.

In this paper, the piecewise parabolic advection (PPA) scheme already developed by the authors to solve the two-dimensional geometry is used equation (5) [34, 42, 44, 45]. The left-hand side of equation (5) is treated by the upwind monotonic interpolation methods. PPA scheme is very efficient and produces very small amount of diffusion. The average computational time is about 2000 s on an alpha workstation with a 633 MHz, 21164 CPU for the discrete ordinate quadrature, 16 × 50 spatial grid at 1000 time steps.

3. Experimental procedure

The experimental set-up for time resolved optical signal measurement as shown in figure 2(*a*). The laser system used for the experiment consists of mode locked argon–ion laser having a pulse width (t_p) = 200 ps at FWHM operating at a repetition rate of 76 MHz (λ = 514 nm). The laser beam is split into two parts: one is used as the time reference and the other is incident to the tissue phantom. A translation stage is introduced for an adjustable optical delay in the reference beam to be used as reference for the determination of the origin of the timescale. The power and pulse width of the laser is monitored throughout the experiment using a power metre and ultra fast photodiode, respectively. The tissue phantom is mounted on

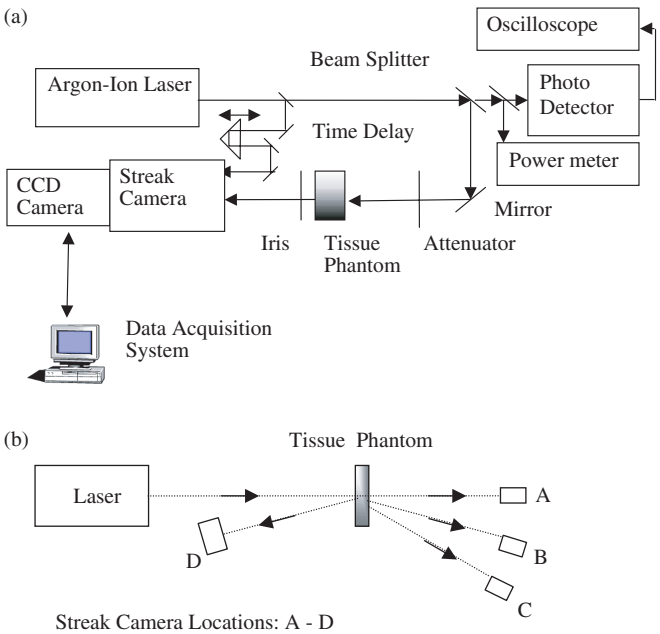

Figure 2. (*a*) Schematic of the experimental set-up. (*b*) Different measurement locations for transmittance (A)–(C) and reflectance (D).

a translation stage. The scattered transmitted and reflected optical signals from the tissue phantoms are collected using a Hamamatsu streak camera unit. Attenuators are used to control incident power on tissue phantoms so as not to saturate the streak camera.

Streak camera is used for direct measurement of scattered optical signals with very high temporal resolution. It simultaneously measures time, position (or wavelength) and light intensity and processes the data in real time using a dedicated read out system. The streak camera used for the experiments is Hamamatsu C1587 and M1954 synchroscan unit along with M1955 frequency tuning unit coupled with a Hamamatsu C4742-95 CCD camera. The incident light on the photocathode is converted into a number of electrons proportional to the intensity of the light, so that the optical pulses are converted sequentially into electrons. They then pass through a pair of accelerating electrodes, where they are accelerated and bombarded against a phosphor screen. The phosphor image corresponding to the optical pulse which was the earliest to arrive is placed in the uppermost position, with the other images being arranged in sequential order from top to bottom; in other words, the vertical direction on the phosphor screen serves as the time axis. The position in the horizontal direction of the phosphor image corresponds to the horizontal location of the incident light. The time resolution of the streak camera used in this study is 10 ps.

4. Results

Experimental investigations of interactions of short-pulsed laser with scattering absorbing media like tissue phantoms containing inhomogeneities are conducted. The results are validated with numerical modelling results obtained by solving a two-dimensional transient RTE using the DOM. The tissue phantoms used are cast by mixing araldite resin having a refractive index (n) of 1.54 together with an anhydride and a hardener. Typical sample cross-section used is 25 mm $\times$ 50 mm with varying thickness of 8 mm and 12 mm. Titanium dioxide (TiO_2) particles having a mean diameter of 0.3 μm is added as scatterers and dye is used as absorbers. The scattering and absorption coefficients are varied by varying the concentration of TiO_2 and dye in the resin matrix [46]. Inhomogeneities typically of 4 mm diameter are drilled in the samples and filled with different scattering and absorption coefficients than the base resin matrix. The set-up is tested with phantoms of different scattering and absorption characteristics. Experiments are conducted on tissue phantoms to measure transmitted and reflected optical signals along the axis of the laser beam as well as at different angles. Line scan is performed for each sample 1 mm apart, and temporal profile for each position is collected over a time window of 2000 ps (2 ns/15 mm of PMT). Standard background subtraction is performed for each measurement. Measurement of these optical signals are performed by analog integration for 200 ms. For numerical simulations a value of $g = 0.8$ [47] is used. The scattering coefficient k_s and anisotropy factor g can be conveniently combined in terms of the transport scatter coefficient $k_s' = k_s\,(1 - g)$. For a phantom of $k_s' = 20\,\mathrm{cm}^{-1}$ and $k_a = 0.5\,\mathrm{cm}^{-1}$ and a thickness of 8 mm, incident power of 100 mW is used. The average output obtained is 58 μW for 8 mm and 5.7 μW for 12 mm, respectively.

Figure 3 shows the normalized transmitted optical signal measurements obtained with a homogenous tissue phantom of thickness (L) = 8 mm and 12 mm, respectively. The tissue phantom having a scattering coefficient (k_s') = $20\,\mathrm{cm}^{-1}$ and absorption coefficient (k_a) = $0.5\,\mathrm{cm}^{-1}$ is used. These optical coefficient values are close to real tissue properties [9, 24, 47]. It is observed that the experimental measurements agree with the numerical simulation results. The time for earliest arriving photon for the 8 mm phantom of refractive index n of 1.54 is

$$\frac{\text{Length of the medium}}{\text{Speed of light in the medium}} = \frac{8 \times 10^{-3}\,\mathrm{m}}{3 \times 10^{8}\,\mathrm{m\,s^{-1}}/1.54} = 41.07\,\mathrm{ps}. \quad (6)$$

The transmission signal values are zero till this time. These values are consistent with both the numerical and experimental measurements as observed in figure 3. Many previously used approximate models fail to capture this effect and provide unrealistic results for the transmitted signals even before light has traversed through the medium. Also as the thickness of the medium is increased from 8 to 12 mm there is a temporal shift in transmitted optical signal with a corresponding increase in pulse width. Repeatibilty in experimental measurements is within $\pm 1\%$ error. Figure 4 shows the corresponding

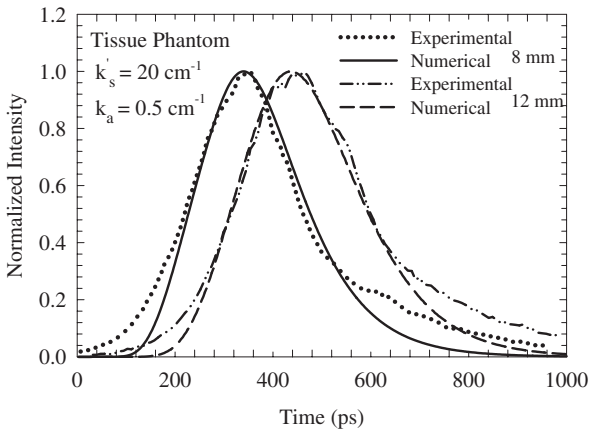

Figure 3. Comparison between numerical models and experimental measurements of the temporal transmitted signal for a tissue phantom.

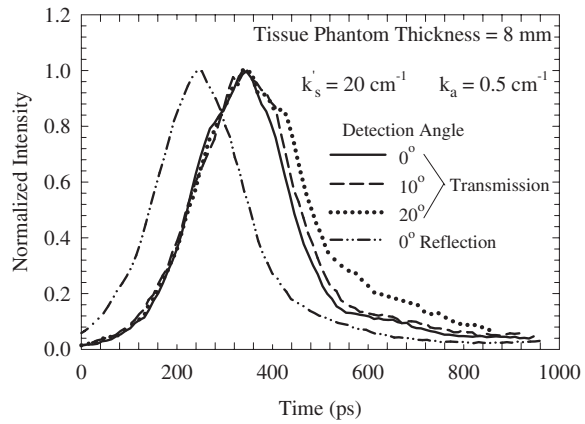

Figure 4. Experimental measurements of temporal scattered signals for a tissue phantom at different detector angles.

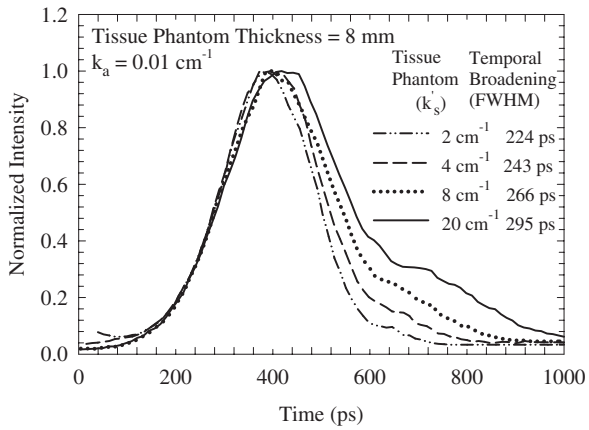

Figure 5. Effect of scattering coefficient on measured transmitted signal for a tissue phantom.

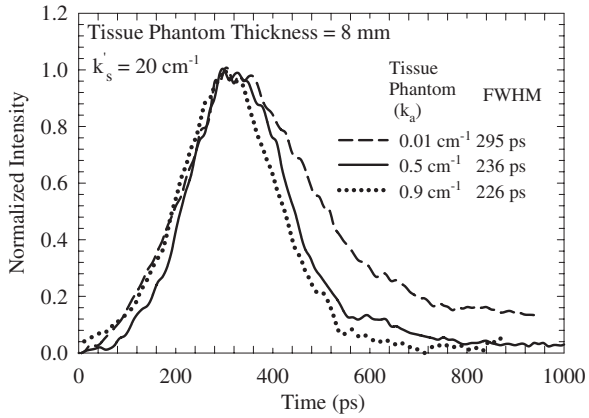

Figure 6. Effect of absorption coefficient on measured transmitted signal for a tissue phantom.

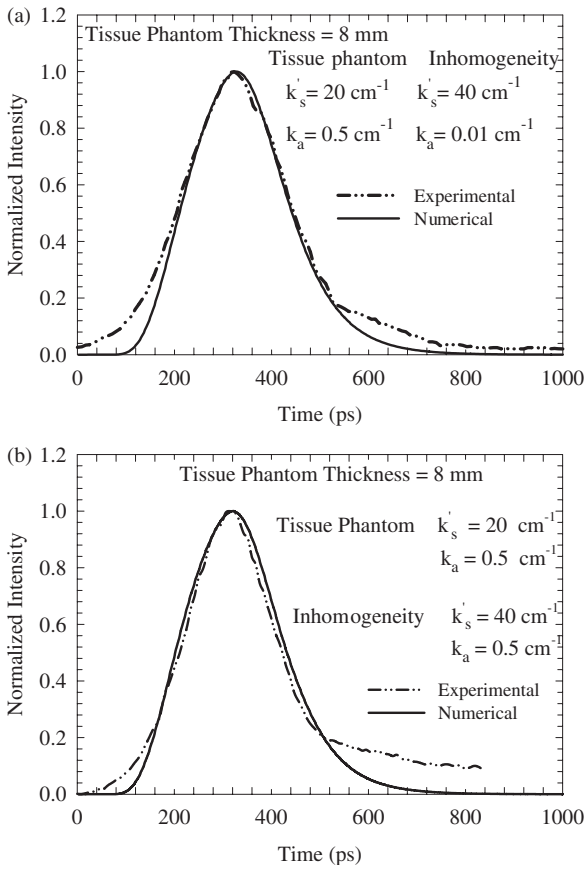

Figure 7. Comparison between numerical models and experimental measurements of the temporal transmitted signal for a tissue phantom containing inhomogeneity for (*a*) inhomogeneity absorption coefficient = 0.01 cm^{-1}, (*b*) inhomogeneity absorption coefficient = 0.5 cm^{-1}.

normalized scattered optical signals for an 8 mm thick tissue phantom for different detector orientations corresponding to figure 2(*b*). The photons measured in the forward direction have higher temporal broadening due to more multiple scattering.

Experiments are conducted by varying the amount of scatterers and therefore the scattering coefficient for the case of 8 mm thick homogeneous tissue phantoms. The normalized temporal transmitted signal profiles are plotted for various scattering coefficients ($k_\mathrm{s} = 2, 4, 8$ and $20\,\mathrm{cm}^{-1}$), keeping the absorption coefficient fixed ($k_\mathrm{a} = 0.01\,\mathrm{cm}^{-1}$). It is observed in figure 5 that the temporal spread increases with the increase of concentration of scatterers in the phantoms (i.e. the scattering coefficients) as the phantoms undergo more multiple scattering. The magnitude of the signal also increases with the increase of the scattering coefficients but is masked due to the normalization with respect to corresponding peak intensity values. The effect of the variation of the absorption coefficient ($k_\mathrm{a} = 0.01, 0.5$ and $0.9\,\mathrm{cm}^{-1}$) of the tissue phantom is depicted in figure 6. Higher the absorption, higher will be the attenuation of the laser beam and hence lower the temporal broadening.

Figure 7(*a*) shows temporal profile of normalized transmitted signal for a tissue phantom containing inhomogeneity. The scattering coefficients of base tissue phantom are different from inhomogeneity which is having higher scattering coefficient ($k'_\mathrm{s} = 40\,\mathrm{cm}^{-1}$) than surrounding base tissue medium ($k'_\mathrm{s} = 20\,\mathrm{cm}^{-1}$). The base medium absorption coefficient ($k_\mathrm{a} = 0.5\,\mathrm{cm}^{-1}$) is significantly higher than that of inhomogeneity ($k_\mathrm{a} = 0.01\,\mathrm{cm}^{-1}$). There is a reasonable match between numerical and experimental value with a little separation in the tail section. This can be attributed to the fact that as absorption coefficient is increased, it decreases number of photons that is collected by the detector at face 2. Further normalization of signal amplifies the noise at the tail of the pulse. This phenomenon is more pronounced in figure 7(*b*) where the inhomogeneity absorption coefficient is increased from $k_\mathrm{a} = 0.01\,\mathrm{cm}^{-1}$ to $k_\mathrm{a} = 0.5\,\mathrm{cm}^{-1}$. The spatial intensity corresponding to figure 7(*a*) along the opposite face of incident radiation (face 2) for different times are plotted in figure 8. At very small and very large times detection of the inhomogeneity is difficult. Within time instant of 300–450 ps, demarcation between base and inhomogeneity is most prominent. Therefore a selection of appropriate time window is critical for maximum contrast between tissue phantom and inhomogeneity. It is observed that optical signals measured very close to the edges showed fluctuations due to boundary effects and hence are not shown in the figure. Numerical results for all time instants match the experimental results, are not shown for purpose of brevity. Figure 9 shows the effect of variation of scattering coefficient ($k'_\mathrm{s} = 30$ and $40\,\mathrm{cm}^{-1}$) and absorption coefficient ($k_\mathrm{a} = 0.01$ and $0.5\,\mathrm{cm}^{-1}$) of the inhomogeneity on the spatial distribution of intensity. The properties of base tissue medium are same as in figure 7(*a*). Typically change in properties

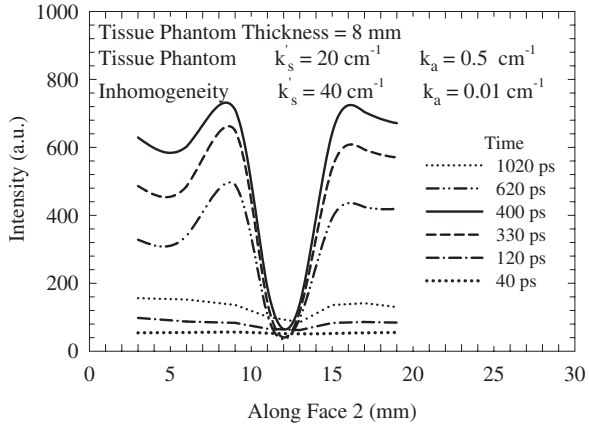

Figure 8. Spatial measurements of intensity distribution in the phantom containing inhomogeneity at different times.

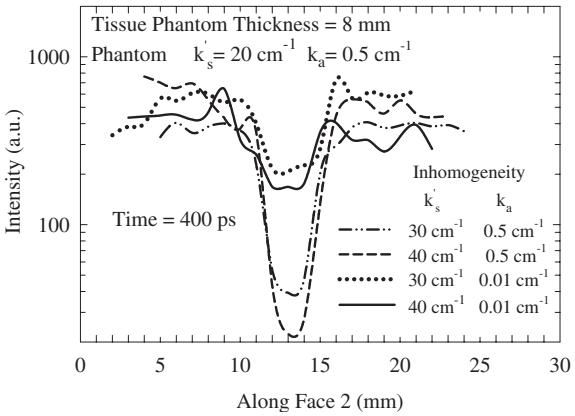

Figure 9. Spatial measurements of intensity distribution in the phantom containing inhomogeneity for different inhomogeneity optical parameters.

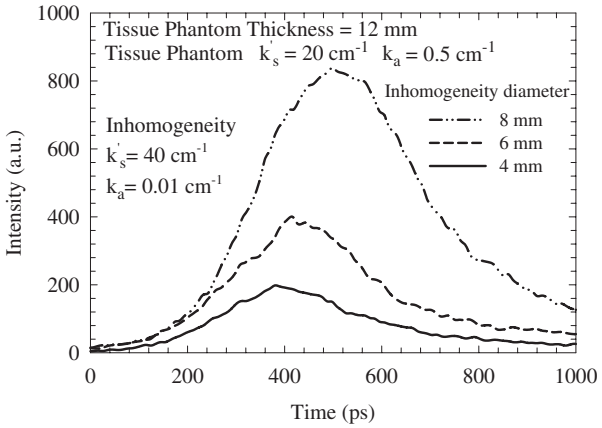

Figure 10. Effect of inhomogeneity size on measured transmitted signal for a tissue phantom containing inhomogeneity.

of tumour is anticipated whereas base tissue properties are fairly constant. The intensity is in arbitrary units as only relative measurements can be done with the streak camera. It is interesting to note that increase of absorption increases the contrast whereas the effect of increase of scattering coefficient is not so pronounced. But at the same time, increase of absorption coefficient decreases the spatial resolution, which again is not the case with increase of scatterers in the inhomogeneity.

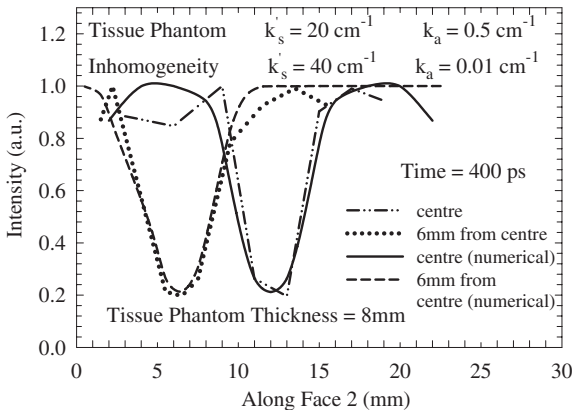

Figure 11. Comparison between numerical models and experimental measurements of the spatial intensity distribution for a tissue phantom containing inhomogeneity.

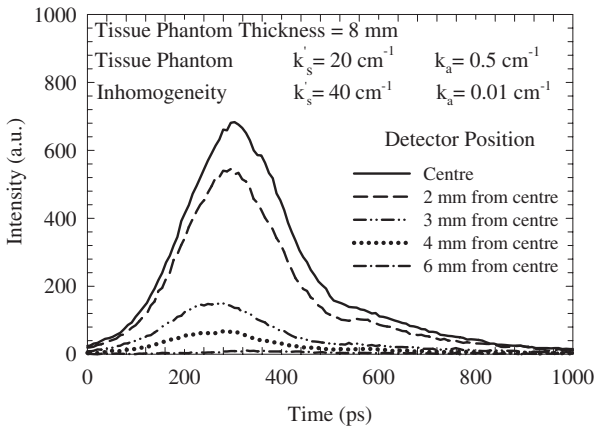

Figure 12. Experimental measurement of transmitted signal at different detector position for a tissue phantom containing inhomogeneity.

Figure 10 depicts the change in intensity of temporal profile due to change of inhomogeneity thickness. This experiment is performed with thicker (12 mm) sample so that different size of inhomogeneities can be drilled. It is evident as the inhomogeneity size increases the temporal broadening of optical signal transmitted out from face 2 increases. Figure 11 depicts the match between numerical model and experimental measurement when inhomogeneity is varied in spatial direction. It is evident from the figure that there is some mismatch which may be due to non-uniform distribution of scatterers during sample preparation.

The effect of the detector position on the transmitted signal obtained is shown in figure 12. From figure 1 it is evident that the centre of the tumour is on the same axis as the detector centre. Therefore the detector position at the centre receives more early arriving photons than the detectors further away from the centre implying presence of some inhomogeneity in the tissue medium.

5. Conclusions

A comprehensive experimental and numerical investigation is performed to analyse short pulse laser propagation through tissue medium having inhomogeneities/tumour imbedded in it. Parametric study as performed in this paper is critical in

order to differentiate between healthy and tumourous tissue. Detection of inhomogenieties depends on optical properties of inhomogenieties compared to base tissue medium. The resolution of spatial detection decreases with increase of absorption coefficient, but at the same time difference in intensity magnitude is high compared to the case when there is increase in scattering coefficient. Also increase in inhomogeneity size changes the temporal intensity profile significantly. Accurate validation of the forward transient RTE with the experimentally measured data is performed in this paper. Short pulse laser probing for detection of tumours in tissues is a novel and nascent technology and this research work can be furthered by experiments on animal models.

Acknowledgments

Kunal Mitra acknowledges partial support from Oak Ridge National Laboratory through Contract No 4000004751. Tuan Vo-Dinh acknowledges support from NIH grant No 1 R01 CA88787-01 and US Department of Energy, Office of Environmental and Biological Research under Contract No DE-AC05-00OR22725 with UT Battelle, LLC.

References

[1] Benaron D A *et al* 2000 Noninvasive functional imaging of human brain using light *J. Cereb. Blood Flow Metab.* **20** 469–77

[2] Grable R J, Rohler D P and Sastry K L A 1997 Optical tomography breast imaging *Proc. SPIE.* **2979** 197–210

[3] Pogue B W, Patterson M S, Jiang H and Paulsen K D 1995 Initial assessment of a simple system for frequency domain diffuse optical tomography *Phys. Med. Biol.* **40** 1709–29

[4] Fantini S, Franceschini M A, Gratton E, Hueber D, Rosenfeld W, Maulik D, Stubblefield P G and Stankovic M R 1999 Non-invasive optical mapping of the piglet in real time *Opt. Express* **4** 308–14

[5] Ntziachristos V, Ma X and Chance B I 1998 Time-correlated single photon counting imager for simultaneous magnetic resonance and near-infrared mammography *Rev. Sci. Instrum.* **69** 4221–33

[6] Barbour R L, Andronica R, Sha Q, Graher H L and Soller I 1998 Development and evaluation of the IRIS-OPTI scanner, a general-purpose optical tomographic imaging system *OSA TOPS* **21** 251–5

[7] Kaschke M, Jess H, Gaida G, Kaltenbach J and Wrobel W 1994 Transillumination imaging of tissue by phase modulation techniques *OSA Proc.* **21** 88–92

[8] Colak S B, Papaioannou D G, 't Hooft G W, van der Mark M B, Schomberg H, Paasschens J C J, Melissen J B M and van Asten N 1997 Tomographic image reconstruction from optical projections in light-diffusing media *Appl. Opt.* **36** 180–213

[9] Grosenick D, Wabnitz H, Rinneberg H H, Moesta T and Schlag P M 1999 Development of a time-domain optical mammography and first *in vivo* applications *Appl. Opt.* **38** 2927–43

[10] Eda H *et al* 1999 Multichannel time-resolved optical tomographic imaging system *Rest Sci. Instrum.* **70** 3595–602

[11] Hillman E C, Hebden J C, Schweiger M, Dehghani H, Schmidt F W, Delpy D T and Arridge S R 2001 Timer-resolved optical tomography of the human forearm *Phys. Med. Biol.* **46** 1117–30

[12] Graber H L, Chang J, Lubowsky J, Aronson R and Barbour R L 1993 Near infrared absorption imaging of dense scattering media by steady-state diffusion tomography *Proc. SPIE* **1888** 372–86

[13] Arridge S R and Schweiger M 1995 Sensitivity to prior knowledge in optical tomographic reconstruction *Proc. SPIE* **2389** 378–88

[14] Mitra K and Kumar S 1999 Development and comparison of models for light pulse transport through scattering absorbing media *Appl. Opt.* **38** 188–96

[15] Hall D J, Hebden J C and Deply D T 1997 Imaging very-low-contrast objects in breastlike scattering media with a time-resolved method *Appl. Opt.* **36** 7270–6

[16] Yoo K M and Alfano R R 1990 Time-resolved coherent and incoherent components of forward light scattering in random media *Opt. Lett.* **15** 320–2

[17] Yoo K M, Das B B, Liu F, Xing Q and Alfano R R 1993 Femtosecond time-gated imaging of translucent objects hidden in highly scattering media *Springer Ser. Chem. Phys.* **55** 124–7

[18] Hebden J C, Kruger R A and Wong K S 1991 Tomographic imaging using picosecond pulses of light *SPIE Proc. Med. Imaging V: Image Phys.* **1443** 294–300

[19] Wang L, Ho P P, Liu C, Zhang G and Alfano R R 1991 Ballistic 2-D imaging through scattering walls using an ultrafast kerr gate *Science* **253** 769–71

[20] Alfano R R, Liang X, Wang L and Ho P P 1994 Time resolved imaging of translucent droplets in highly scattering turbid media *Science* **264** 1913–15

[21] Berg R, Andersson-Engels S, Jorlman O and Svanberg S 1991 Time-resolved transillumination for medical diagnostics *SPIE Proc.* **1431** 110–19

[22] Huang D *et al* 1991 Optical coherence tomography *Science* **254** 1178–81

[23] Hebden J C 1992 Evaluating the spatial resolution performance of time-resolved optical imaging system *Med. Phys.* **19** 1081–7

[24] Hebden J C and Arridge S R 1996 Imaging through scattering media by the use of an analytical model of perturbation amplitudes in the time domain *Appl. Opt.* **35** 6788–95

[25] Hielscher A H, Catarious D M, Klose A and Hanson K M 1998 Tomographic imaging of brain and breast tissue by time-resolved model-based iterative image reconstruction *Proc. Advances in Optical Imaging and Photon Migration* pp 125–7

[26] Arridge S R 1993 The forward and inverse problem in time resolved infrared imaging *Medical Optical Tomography: Functional Imaging and Monitoring* ed G Muller (Bellingham: SPIE Press)

[27] Singer J R, Grunbaum F A, Kohn P and Zubelli J P 1990 Image reconstruction of the interior of bodies that diffuse radiation *Science* **248** 990–1

[28] Jiang H, Paulsen K D, Osterberg U L, Pogue B W and Patterson M S 1995 Simultaneous reconstruction of optical absorption and scattering maps in turbid media from near-infrared frequency-domain data *Opt. Lett.* **20** 2128–30

[29] Gratton E, Mantulin W M, vande Ven M J, Fishkin J B, Maris M B and Chance B 1993 A novel approach to laser tomography *Bioimaging* **1** 40–6

[30] Berndt K W and Lakowicz J R 1991 Detection and localization of absorbers in scattering media using frequency domain principles *SPIE Proc.* **1431** 149–60

[31] O'Leary M A, Boas D A, Chance B and Yodh A G 1995 Experimental images of heterogeneous turbid media by frequency domain diffusing photon tomography *Opt. Lett.* **20** 426–8

[32] Brewester M Q and Yamada Y 1995 Optical properties of thick turbid media from picosecond time-resolved light scattering measurement *Inter. J. Heat Mass Transfer* **8** 2569–81

[33] Ishimaru A 1989 Diffusion of light in turbid material *Appl. Opt.* **28** 2210–15

[34] Sakami M, Mitra K and Vo-Dinh T 2002 Analysis of short-pulse laser photon transport through tissues for optical tomography *Opt. Lett.* **27** 336–8

[35] Sakami M, Mitra K and Hsu P 2000 Transient radiative transfer in anisotropically scattering media using monotonicity-preserving schemes *International Mechanical Engineering Congress and Exposition* vol 366-1, pp 135–43
[36] Kumar S, Mitra K and Yamada Y 1996 Hyperbolic damped-wave models for transient light-pulse propagation in scattering media *Appl. Opt.* **35** 3372–8
[37] Mitra K, Lai M S and Kumar S 1997 Transient radiation transport in participating media within a rectangular enclosure *AIAA J. Thermophys. Heat Transfer* **11** 409–14
[38] Tan Z M and Hsu P 2001 An integral formulation of transient radiative transfer *ASME J. Heat Transfer* **123** 466–75
[39] Wu C Y and Wu S H 2000 Integral equation formulation for transient radiative transfer in an anisotropically scattering medium *International J. Heat Mass Transfer* **43** 2009–20
[40] Gandbakche A H, Nossal R and Bonner R F 1993 Scaling relationships for theories of anisotropic random walks applied to tissue optics *Appl. Opt.* **32** 504–16
[41] Sawetprawichkul A, Hsu P, Mitra K and Sakami M 2000 A Monte Carlo study of the transient radiative transfer within the one-dimensional multi-layered slab *International Mechanical Engineering Congress and Symp. (Orlando, FL)* vol 366-1, pp 145–53
[42] Sakami M, Mitra K and Hsu P 2002 Analysis of light-pulse transport through two-dimensional scattering-absorbing media *J. Quant. Spectrosc. Radiat. Transfer* **73** 169–79
[43] Modest M F 1993 *Radiative Heat Transfer* (New York: McGraw Hill)
[44] Strang G 1968 On the construction and comparison of difference schemes *SIAM J. Numer. Ann.* **5** 506–17
[45] Colella P and Woodward P R 1984 The piecewise parabolic method for gas-dynamical simulations *J. Comput. Phys.* **54** 174–201
[46] Firbank M and Delpy D T 1993 A design for a stable and reproducible phantom for use in near infra-red imaging and spectroscopy *Phys. Med. Biol.* vol 38, pp 847–85
[47] Jarlman O, Berg R, Andersson-Engels S, Svanberg S and Pettersson H 1997 Time-resolved white light transillumination for optical imaging *Acta Radiologica* **38** 185–9